

A multiresolution Discrete Element Method for triangulated objects with implicit timestepping

Peter Noble Tobias Weinzierl

November 18, 2021

Abstract

Simulations of many rigid bodies colliding with each other sometimes yield particularly interesting results if the colliding objects differ significantly in size and are non-spherical. The most expensive part within such a simulation code is the collision detection. We propose a family of novel multiscale collision detection algorithms that can be applied to triangulated objects within explicit and implicit time stepping methods. They are well-suited to handle objects that cannot be represented by analytical shapes or assemblies of analytical objects. Inspired by multigrid methods and adaptive mesh refinement, we determine collision points iteratively over a resolution hierarchy, and combine a functional minimisation plus penalty parameters with the actual comparison-based geometric distance calculation. Coarse surrogate geometry representations identify “no collision” scenarios early on and otherwise yield an educated guess which triangle subsets of the next finer level potentially yield collisions. They prune the search tree, and furthermore feed conservative contact force estimates into the iterative solve behind an implicit time stepping. Implicit time stepping and non-analytical shapes often yield prohibitive high compute cost for rigid body simulations. Our approach reduces these cost algorithmically by one to two orders of magnitude. It also exhibits high vectorisation efficiency due to its iterative nature.

1 Introduction

The simulation of rigid bodies or rigid body parts is a challenge that arises in many fields. Notably, it is at the heart of Discrete Element simulations (DEM), where millions of these objects are studied. Progress on simulations with rigid, impenetrable objects depends on whether we can handle high geometric detail: For the analysis of particle flow such as powder, it is mandatory to simulate billions of particles, while the realism of some simulations hinges on the ability to handle particles of different shapes and sizes. It is the support of different shapes and sizes that allows us to simulate complex mixture and separation of scales phenomena, or blockage if many objects, aka particles, try to squeeze through narrow geometries, e.g.

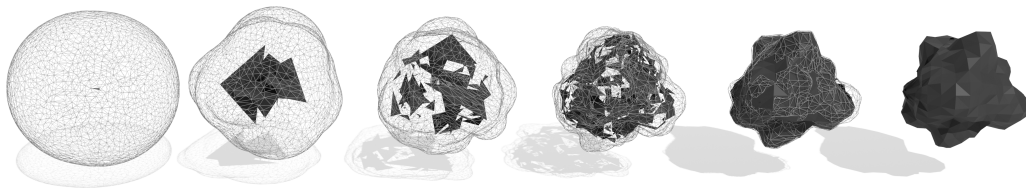


Figure 1: Surrogate triangle hierarchy for a “bumped sphere”. The actual sphere geometry \mathbb{T}_h is shown on the right. From right to left: Coarser and coarser surrogate representations incl. their ϵ -environments. The coarser a representation, the lower the triangle count and the larger the corresponding ϵ . The surrogate triangles are weakly connected.

DEM codes spend most of their runtime on collision detection [8, 10, 11, 13]—even if they restrict to analytical shapes only. We tighten the challenge and study a DEM prototype over particles where (i) rigid particles have massively differing size, (ii) rigid particles are discretised by many triangles, and (iii) rigid particles have complicated, non-convex shapes. Our code supplements each rigid particle with an ϵ -area and considers two particles to be “in contact” if their ϵ -environment overlaps. This yields a weak compressibility model, where the contact points are unique up to an ϵ -displacement. Both the arrangement and the topology of these points can change significantly between any two time steps, while the collision models using the contact data are inherently stiff.

Our work proposes a multiscale contact detection scheme which brings down the compute time for the contact detection aggressively. We can handle complex, non-convex shapes and even speed up implicit time stepping significantly. The latter is, so far, prohibitively expensive for most codes. To reduce the runtime, our approach phrases the contact search as an iterative algorithm over multiple resolutions where coarser particle resolutions act as surrogates. This idea enables us to introduce five algorithmic optimisations: First, the surrogates help us to identify “no contact” constellations quickly. Second, they exploit that we do not represent surrogate resolutions as a plain level of detail [1] but make them form a tree: If we identify a potential collision, only those sections of the geometry are “up-pixelated” from where a collision point might arise from. We increase the resolution locally. Third, the surrogate resolutions yield conservative estimates of the force that might result from a contact point. Once we employ an implicit time stepping scheme with a Picard iteration, we can permute the iterative solver loop and the resolution switches such that the Picard iteration forms the outer loop which zaps through resolution levels upon demand. Fourth, we phrase the contact detection as a distance minimisation problem [9, 10]. The minimisation problem is solved iteratively through an additional, embedded Newton which approximates the Jacobian via a diagonal matrix and runs through a prescribed number of sweeps. Once more, we permute the loop over triangle pairs and Picard iterations to improve the vectorisation suitability. Finally, we acknowledge that an iterative minimisation subject to a prescribed iteration count can fail if the underlying geometric problem is ill-posed. In such cases, we eventually postprocess it by falling back to a comparison-based distance calculation. However, this is only required on the finest mesh, whereas we use non-convergence within the surrogate tree as sole “refinement criterion” (use a finer mesh) that does not contribute forces towards the implicit time stepping.

To the best of our knowledge, our rigorous multiscale idea, which can be read as a combination of (i) loop permutation and fusion, (ii) adaptive mesh refinement, (iii) a generalisation of volume bounding hierarchies [2, 3, 4, 6, 7] and (iv) an approximate, weak closest-triangle formulation [9, 10], is unprecedented. Its reduction of computational cost plus its excellent vectorisation character in combination with the fact that rigid body simulations scale well by construction—the extremely short-range interactions fit well to domain decomposition—brings implicit DEM simulations for triangulated, non-convex shapes within practical applications into reach. The core algorithmic ideas furthermore have an impact well beyond the realm of DEM. The search for nearest neighbours, i.e. contact within a certain environment, is, for example, also a core challenge behind fluid-structure interaction (FSI).

The manuscript is organised as follows: We first introduce our algorithmic challenge and a textbook implementation of both explicit and implicit time stepping for it (Section 2). An efficient contact detection between triangulated surfaces of two particles via a minimisation problem is introduced next (Section 3), before we rewrite the underlying geometric problem as a multiresolution challenge and introduce our notion of a surrogate data structure (Section 4). In Section 5, we bring both the efficient triangle comparisons and the tree idea together as we plug them into an implicit time stepping code, before we allow the non-linear equation system solvers’ iterations to move up and down within the surrogate tree. This is the core contribution of the manuscript. Following the discussion of some numerical results (Section 6), we sketch future work and close the discussion.

2 Algorithmic framework

We study a system of $|\mathbb{P}|$ rigid bodies (particles). Each particle $p \in \mathbb{P}$ has a position $x(p, t)$, a velocity $v(p, t)$ and a rotation $r(p, t)$. Each is described by a triangular tessellation $\mathbb{T}(p, t)$. $t \geq 0$ is the simulation time. We may assume that $\mathbb{T}(p, t)$ spans a well-defined, closed surface represented by a conformal mesh: No two triangles intersect, two triangles share at most one complete edge or exactly one vertex, and we can “run around” a particle infinitely often without falling into a gap. While the triangulation of the object is time-invariant, it moves and rotates over time and therefore depends on t .

Algorithm 1 High-level pseudo code for an explicit Euler for rigid particles. The continuous properties $v(p, t), r(p, t)$ and $\mathbb{T}(p, t)$ are discretised in time and thus become $v(p), r(p)$ and $\mathbb{T}(p)$. t is the (discretised) time, Δt the time step size.

```

1: while  $t < T_{\text{terminal}}$  do
2:    $\forall p_i \in \mathbb{P} : \mathbb{C}(p_i) \leftarrow \emptyset$ 
3:   for  $p_i, p_j \in \mathbb{P}, p_i \neq p_j$  do
4:      $\mathbb{C}(p_i) \leftarrow \mathbb{C}(p_i) \cup \text{FINDCONTACTS}(\mathbb{T}(p_i), \mathbb{T}(p_j))$ 
5:      $\mathbb{C}(p_j) \leftarrow \mathbb{C}(p_j) \cup \text{FINDCONTACTS}(\mathbb{T}(p_i), \mathbb{T}(p_j))$ 
6:   end for
7:   for  $p_i \in \mathbb{P}$  do
8:      $\mathbb{T}(p_i) \leftarrow \text{UPDATE}(\mathbb{T}(p_i), v(p_i), r(p_i), \Delta t)$ 
9:   end for
10:  for  $p_i \in \mathbb{P}$  do
11:     $(dv, dr) \leftarrow \text{CALCFORCES}(\mathbb{C}(p_i))$ 
12:     $(v, r)(p_i) \leftarrow (v, r)(p_i) + \Delta t \cdot (dv, dr)$ 
13:  end for
14:   $t \leftarrow t + \Delta t$ 
15: end while

```

\triangleright We simulate over a time span
 \triangleright Clear set of collisions for particle p_i
 \triangleright Run over all particle pairs
 \triangleright Update geometry
 \triangleright using velocity, rotation and time step size
 \triangleright Update velocity and rotation

Algorithm 2 Contact identification between two particles p_i and p_j .

```

1: function  $\text{FINDCONTACTS}(\mathbb{T}(p_i), \mathbb{T}(p_j))$ 
2:    $\mathbb{C} = \emptyset$ 
3:   for  $t_i \in \mathbb{T}(p_i), t_j \in \mathbb{T}(p_j)$  do
4:      $c \leftarrow \text{CONTACT}(t_i, t_j)$ 
5:     if  $c \neq \perp$  then
6:        $\mathbb{C} \leftarrow \mathbb{C} \cup \{c\}$ 
7:     end if
8:   end for
9:   return  $\mathbb{C}$ 
10: end function

```

\triangleright Run over all triangles pairs
 \triangleright Find closest point in-between t_i and t_j and compare normal
 $\triangleright |n|$ against ϵ ; return \perp if $|n| > \epsilon$

Time stepping A straightforward high-level implementation of an explicit Euler for DEM consists of a time loop hosting a sequence of further loops (Algorithm 1): The first inner loop identifies all contact points between the particles. Once we know all contact points per particle, we can determine a velocity and rotation update ($dv(p)$ and $dr(p)$) per particle. Before we do so, we update the particles’ positions using their velocity and angular momentum. Finally, we progress in time. Euler-Cromer would result from a permutation of the update sequence.

It is impossible to simulate exact incompressibility with explicit time stepping schemes: Everytime we update a particle, we run risk that it slightly penetrates another one due to the finite time step size Δt . At the same time, particles exchange no momentum as long as they are not in direct contact yet. The momentum exchange remains “trivial” until we have violated the rigid body constraint. For these two reasons, we switch to a weak incompressibility model where each particle is surrounded by an $\epsilon > 0$ area. The area is spanned by the Minkovski sum of the triangles from $\mathbb{T}(p, t)$ and a sphere of radius ϵ minus the actual rigid object. Without loss of generality, we assume a uniform ϵ per particle. Our formalism is equivalent to a soft boundary formulation with an extrusive surface.

Definition 1 (Contact point) *Each particle is surrounded by an ϵ -environment. Two particles are in contact, if their ϵ -environment overlaps. Overlaps yield contact points which in turn yield forces.*

We parameterise each contact point with its penetration depth: Our contact detection in Algorithm 2 identifies the closest path between two triangles. A potential contact point c is located at the centre of this line. It furthermore is equipped with a normal $n(c)$ which points along the line towards either of the closest triangle (Figure 2). There is an overlap between the two ϵ -augmented triangles if and only if $|n(c)| \leq \epsilon$. Such a point c is added to the set of collision points.

With a set of contact points plus their normals, we can derive a force acting on a particle and, taking the centre of mass and the mass of a particle into account, determine its acceleration and torque [?]. We compute forces by modelling the ϵ -area as a simple spring with a perpendicular friction force. This is a simplistic presentation—we ignore for example sophisticated interaction functions which distinguish contact points from contact faces—yet it allows us to focus on the core challenge how to find contact points efficiently.

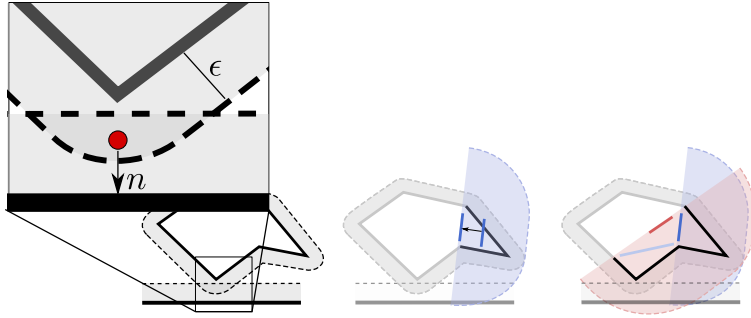


Figure 2: A pair of objects (black, solid) with their ϵ -environment (black, dotted) collide. In the present sketch, one object is a “spherical” particle spanned by six edges, while the other object is a plane at the bottom. Left: Two-dimensional sketch of the contact point concept. The zoom-in shows the contact point which is located in the middle of the overlap region. The contact normal is directed from the middle point towards the closest point on one of the objects involved. Middle: When an object hosts very extruded features, we slightly shrink the surrogate such that the surrogate without ϵ becomes a closer fit around the “un-bumped” real geometry. We trade such a surrogate for a bigger ϵ . Empirical evidence suggests that this yields slightly advantageous forces within a multiscale iterative solve. Right: The conservative property of the surrogate triangles states that all fine level geometry (including its epsilon boundary) must be encompassed by the surrogate’s epsilon. This doesn’t suggest that all surrogate children are included.

Semi-implicit time stepping An implicit Euler for this challenge has to solve a non-trivial, non-linear equation system per time step. Non-trivial means that the system’s sparsity pattern depends on the solution of the system itself. It is determined by the contact point search: we obtain entries in the interaction matrix where the corresponding normal $|n| \leq \epsilon$. Non-linearity means that the quantities in the interaction matrix (forces) depend on the (guess of the) geometries’ arrangement.

Assumption 1 *Our implicit time stepping problem exhibits a contraction property, i.e. Picard iterations can solve the underlying non-linear equation system.*

As our non-linear system is “well-behaved”—we employ reasonably small Δt —we rely on a fixed-point formulation of the implicit timestepping and employ Picard iterations, i.e. we approximate the velocity and rotation $(dv, dr)(p)(t)$ through a repeated application of the contact detection plus its following force calculation (Algorithm 3). We assume that we remain within the Picard iterations’ region of convergence.

Algorithm 3 High-level pseudo code for an implicit Euler.

```
1: while  $t < T_{\text{terminal}}$  do ▷ We simulate over a time span
2:    $\forall p_i \in \mathbb{P} : \mathbb{T}^{\text{guess}}(p_i) \leftarrow \mathbb{T}(p_i), v^{\text{guess}}(p_i) \leftarrow v(p_i), r^{\text{guess}}(p_i) \leftarrow r(p_i)$ 
3:   while  $\mathbb{T}^{\text{guess}}, v^{\text{guess}}$  or  $r^{\text{guess}}$  change significantly for any  $p \in \mathbb{P}$  do
4:      $\forall p_i \in \mathbb{P} : \mathbb{C}(p_i) \leftarrow \emptyset$  ▷ Clear set of collisions for particle  $p_i$ 
5:     for  $p_i, p_j \in \mathbb{P}, p_i \neq p_j$  do ▷ Run over all particle pairs
6:        $\mathbb{C}(p_i) \leftarrow \mathbb{C}(p_i) \cup \text{FINDCONTACTS}(\mathbb{T}^{\text{guess}}(p_i), \mathbb{T}^{\text{guess}}(p_j))$ 
7:        $\mathbb{C}(p_j) \leftarrow \mathbb{C}(p_j) \cup \text{FINDCONTACTS}(\mathbb{T}^{\text{guess}}(p_i), \mathbb{T}^{\text{guess}}(p_j))$ 
8:     end for
9:     for  $p_i \in \mathbb{P}$  do
10:       $(dv, dr) \leftarrow \text{CALCFORCES}(\mathbb{C}(p_i))$ 
11:       $(v^{\text{guess}}, r^{\text{guess}})(p_i) \leftarrow (v, r)(p_i) + \Delta t \cdot (dv, dr)$ 
12:       $\mathbb{T}^{\text{guess}}(p_i) \leftarrow \text{UPDATE}(\mathbb{T}(p_i), v^{\text{guess}}(p_i), r^{\text{guess}}(p_i), \Delta t)$ 
13:    end for
14:  end while
15:   $\forall p_i \in \mathbb{P} : \mathbb{T}(p_i) \leftarrow \mathbb{T}^{\text{guess}}(p_i), v(p_i) \leftarrow v^{\text{guess}}(p_i), r(p_i) \leftarrow r^{\text{guess}}(p_i)$ 
16:   $t \leftarrow t + \Delta t$ 
17: end while
```

Picard avoids the assembly and inversion of an equation system. However, many contact points enter the algorithm temporarily throughout the iterations, which eventually are not identified as contacts. This happens, for example, if we rotate the particles “too far” throughout the iterations. Despite small Δt , we cannot provide an upper bound on the number of Picard iterations required or make assumptions on the (temporarily) identified contact points, i.e. the cost per iteration.

Notation and terminology Any particle $p \in \mathbb{P}$ has a (closed) volume $V(p)$ which is spanned by its triangular surface $\mathbb{T}(p)$. Since we stick to explicit and implicit single-step, single shot methods, we omit the parameterisation (t) from hereon.

$$p_1 \cap p_2 = \emptyset \quad \forall p_1, p_2 \in \mathbb{P} \text{ with } p_1 \neq p_2,$$

as we have rigid, non-penetrating objects. Consequently, $\mathbb{T}(p_1) \cap \mathbb{T}(p_2) = \emptyset$. The particles’ triangles do not intersect. Yet, as each particle is surrounded by an ϵ -layer, our particles’ triangles $t \in \mathbb{T}(p)$ unfold into a set of volumetric objects $t^\epsilon \in \mathbb{T}^\epsilon(p)$, and our particles’ volumes are extended $p \subset p^\epsilon$, too. Overlaps between extended volumes do exist and yield contact points:

$$p_1^\epsilon \cap p_2^\epsilon \neq \emptyset \Rightarrow \text{contact point} \tag{1}$$

which is equivalent to

$$\exists t_1 \in \mathbb{T}(p_1), t_2 \in \mathbb{T}(p_2) : t_1^\epsilon \cap t_2^\epsilon \neq \emptyset \Rightarrow \text{contact point.}$$

A contact point c between two triangles t_i and t_j in (1) is located at

$$x(c) = \frac{1}{2}(t_1(a_1, b_1) + t_2(a_2, b_2)) \text{ with } \arg \min_{a_1, b_1, a_2, b_2 \in [0,1]} \frac{1}{2} \|t_1(a_1, b_1) - t_2(a_2, b_2)\|^2, \tag{2}$$

if t_1 and t_2 are surrounded by the same ϵ halo. For different ϵ s, the weights for $x(c)$ have to be adapted accordingly. a_1, b_1 are Barycentric coordinates within t_1 , i.e. $t_1(a_1, b_1)$ returns a position within the triangle. a_2 and b_2 are the counterparts for t_2 . If $x(c)$ is the position of the contact point c , the corresponding normal $n(c) = t_1(a_1, b_1) - x(c)$ or $n(c) = t_2(a_2, b_2) - x(c)$.

3 Iterative contact detection via distance minimisation

To find the closest point between two triangles is a classic computational geometry problem [5]. We rely on three different algorithms to identify it:

Direct distance calculation (comparison-based) A comparison-based identification of contact points consists of two steps. First, we compute the distance from each vertex of the two triangles to the closest point on the other triangle as well as the distance between each pair of edges between the two triangles [5]^{PN}. This yields six point-to-triangle distance tests and nine edge-to-edge distance tests. In a second step, we select the minimum distance out of the 15 combinations. This *brute force* calculation yields an exact solution—agnostic of truncation errors—yet requires up to 30+14 comparisons (if statements) per triangle pair, which we tune via masking, blending and early termination [14].

Iterative distance calculation As an alternative to a comparison-based approach, we replace the geometric checks with a functional where we minimise the distance between the two planes spanned by the triangles but add the admissibility conditions over the Barycentric coordinates as Lagrangian parameters [9, 10]. In line with (2), let $a, b \in [0, 1]$ describe any point on their respective triangle:

$$\arg \min_{a_1, b_1, a_2, b_2} J(a_1, b_1, a_2, b_2) := \arg \min_{a_1, b_1, a_2, b_2} \underbrace{\frac{1}{2} \|t_i(a_1, b_1) - t_j(a_2, b_2)\|^2}_{=: \hat{J}(a_1, b_1, a_2, b_2)} + \alpha_{\text{iterative}} \left(\max(0, a_1 - 1) + \min(-a_1, 0) + \max(0, b_1 - 1) + \dots \right). \quad (3)$$

This is a weak formulation of the challenge, since it allows the closest distance line between two triangles to be rooted slightly outside the very triangles.

The minimisation problem can be solved via Newton iterations. However, the arising Hamiltonian becomes difficult to invert or non-invertible for close-to-parallel or actually parallel triangles. We therefore regularise it by adding a diagonal matrix. After that, we approximate the regularised Hamiltonian and update the minimisation and constraints alternately:

$$\begin{aligned} (a_1, b_1, a_2, b_2)^{(n+0.5)} &= (a_1, b_1, a_2, b_2)^{(n)} - \text{diag}^{-1} \left(\hat{H}(a_1, b_1, a_2, b_2)^{(n)} \right. \\ &\quad \left. + \alpha_{\text{regulariser}} \text{id} \nabla_{a_1, b_1, a_2, b_2} \hat{J}(a_1, b_1, a_2, b_2)^{(n)} \right) \\ (a_1, b_1, a_2, b_2)^{(n+1)} &= (a_1, b_1, a_2, b_2)^{(n+0.5)} - \text{diag}^{-1} \left(\tilde{H}(a_1, b_1, a_2, b_2)^{(n+0.5)} \right. \\ &\quad \left. + \alpha_{\text{regulariser}} \text{id} \nabla_{a_1, b_1, a_2, b_2} \tilde{J}(a_1, b_1, a_2, b_2)^{(n+0.5)} \right) \end{aligned}$$

$\alpha_{\text{regulariser}} > 0$ is small, while (n) is the iteration index. The \hat{J} and its Hamiltonian correspond to the quadratic term of the actual functional in (3) aka (2). \tilde{J} and its Hamiltonian cover the remaining penalty terms, i.e. $J - \hat{J}$. However, we omit the Dirac jump terms in there, i.e. we explicitly drop terms that enter the formulae for $a_1 = 0, a_1 = 1, b_1 = 0, \dots$. Our solver iterates back and forth between the \hat{J} -minimisation and a fulfillment of the constraints. This modified Newton becomes a gradient descent, where an approximate step size is adaptively chosen by analysing an approximation of the inverse to the Hamiltonian.

Hybrid distance calculation If two subsequent iterates $|J(a_1, b_1, a_2, b_2)^{(n+1)} - J(a_1, b_1, a_2, b_2)^{(n)}| < C\epsilon$ we have found an actual minimum over functional (3) and can terminate the minimisation. In this case, we assume that a_1, b_1, a_2, b_2 identify the minimum distance. Without further analysis, it is impossible to make a statement on the upper bound on n . Our hybrid algorithm therefore eliminates the termination criterion and imposes $n \leq N_{\text{iterative}}$. Consequently, it labels a distance calculation as invalid if $|J(a_1, b_1, a_2, b_2)^{(N_{\text{iterative}})} - J(a_1, b_1, a_2, b_2)^{(N_{\text{iterative}}-1)}| > C\epsilon$. The iterative code’s result realises a three-valued logic: “found a contact point”, “there is no contact”, or “has not terminated” (Algorithm 4).

Our hybrid algorithm relies upon this iterative building block. It first invokes the modified iterative algorithm. If the result equals “not terminated” ($r = \odot$), the hybrid algorithm falls back to the comparison-based distance calculation. It is thus not really a third algorithm to find a contact point, but a combination of the iterative scheme with the comparison-based approach serving as a posteriori limiter.

Triangle meshes are typically held as graphs over vertex sets. We flatten this graph prior to the contact detection: A sequence of $|\mathbb{T}|$ triangles is converted into a sequence of $3 \cdot 3 \cdot |\mathbb{T}|$

floating point values, i.e. each triangle is represented by the coordinates (three components) of its three vertices. Such a flat data structure can be generated once prior to the contact detection as soon as we know a particle’s position and orientation in space. All topology is lost in this representation and vertex data is replicated—it is a triangle soup—but the data is well-suited to be streamed through vector processing units.

Algorithm 4 A reformulation of the iterative distance calculation. The iterative blueprint (top) is tiled and the early convergence stopping criteria is removed to rewrite it into a version that vectorises more aggressively (bottom). Let $\mathbb{T}_k(p_j)$ pick the k th set of N_{batch} triangles from $\mathbb{T}(p_j)$. r is a result value that holds for each triangle combination either the Barycentric coordinates if they yield a contact point, or \perp if they yield no contact point, or \odot if the triangle combination has to be postprocessed with the comparison-based algorithm.

```

1: for  $t_i \in \mathbb{T}(p_i)$  do
2:   for  $t_j \in \mathbb{T}(p_j)$  do
3:      $a_1, b_1, a_2, b_2, n \leftarrow 0$ 
4:      $J_{\text{old}} \leftarrow \infty; J = J(a_1, b_1, a_2, b_2)$ 
5:     while  $|J - J_{\text{old}}| > C\epsilon \wedge n \leq N_{\text{iterative}}$  do
6:        $J_{\text{old}} \leftarrow J$ 
7:       update  $a_1, b_1, a_2, b_2$  ▷ Modified gradient descent
8:        $n \leftarrow n + 1$ 
9:     end while
10:  end for
11:   $r(t_i, t_j) \leftarrow \begin{cases} (a_1, b_1, a_2, b_2) & \text{if } |J - J_{\text{old}}| \leq C\epsilon \wedge \hat{J} \leq 2\epsilon^2 \\ \perp & \text{if } |J - J_{\text{old}}| \leq C\epsilon \wedge \hat{J} > 2\epsilon^2 \\ \odot & \text{otherwise} \end{cases}$ 
12: end for
13:
14: for  $t_i \in \mathbb{T}(p_i)$  do
15:   for  $0 \leq k < |\mathbb{T}(p_j)|/N_{\text{batch}}$  do
16:      $\forall l \in \{0, \dots, N_{\text{batch}} - 1\} : J_{\text{old},l} \leftarrow \infty; J_l = J(a_{1,l}, b_{1,l}, a_{2,l}, b_{2,l})$ 
17:     for  $0 \leq n < N_{\text{iterative}}$  do
18:        $\forall l \in \{0, \dots, N_{\text{batch}} - 1\} : J_{\text{old},l}(t_j) \leftarrow J_l$  ▷  $N_{\text{batch}}$  concurrent backups of  $J$ 
19:        $\forall l \in \{0, \dots, N_{\text{batch}} - 1\} : \text{update } (a_{1,l}, b_{1,l}, a_{2,l}, b_{2,l})$  ▷  $N_{\text{batch}}$  concurrent gradient steps
20:     end for
21:      $\forall l \in \{0, \dots, N_{\text{batch}} - 1\} : r(t_i, t_j) \leftarrow (\text{see above})$  ▷  $t_j$  is the  $l$ th triangle in current batch
22:   end for
23: end for

```

Let \mathbb{T}_i and \mathbb{T}_j be two triangle sets that have to be compared. To improve the vector efficiency, we tile one of the input triangle sets into batches of size N_{batch} (Algorithm 4). N_{batch} is chosen such that it fits to the vector register width. We next exploit the fact that the iteration count is bounded or hardcoded—i.e. we omit an early termination criterion—and consequently permute the loop over the comparison triangles and the modified Newton iterations. As we compute the result for N_{batch} triangle combinations in one embarrassingly parallel rush, we can vectorise aggressively.

4 A multiresolution model

The cost to compare two particles p_i and p_j is determined by their triangle counts $|\mathbb{T}_i|$ and $|\mathbb{T}_j|$. To reduce this cardinality, we construct geometric cascades of triangle models per particle—the *surrogate models* (Fig. 1)—and plug representations from this cascade into Algorithm 2.

Definition 2 A surrogate model $\mathbb{T}_k(p)$, $k \geq 1$ is a triangle-based geometric approximation of a particle described by $\mathbb{T}(p)$. A sequence of surrogate models $\mathbb{T}_k(p)$ for p with its volumetric extensions $\mathbb{T}_k^\epsilon(p)$ hosts efficient (Definition 3), conservative (Definition 4), and weakly connected (Definition 5) abstractions of $\mathbb{T}(p)$.

Surrogate models are different representations of a particle. They can step in for our real geometry and are a special class of bounding volume techniques [5]. To simplify our notation, $\mathbb{T}_0(p) := \mathbb{T}(p)$. Furthermore, we emphasise that the ϵ is a generic symbol, i.e. each surrogate model hosts its own, bespoke ϵ -environment.

Definition 3 A surrogate model $\mathbb{T}_{k_i}(p_i)$ is efficient if, for any other model $\mathbb{T}_{k_j}(p_j)$, finding all contact points between $\mathbb{T}_{k_i}(p_i)$ and $\mathbb{T}_{k_j}(p_j)$ is cheaper than finding all contact points between $\mathbb{T}_{\hat{k}_i}(p_i)$ and $\mathbb{T}_{k_j}(p_j)$ for all $0 \leq \hat{k}_i < k_i$.

We assume an almost homogeneous cost per triangle-to-triangle comparison—an assumption that is shaky for the hybrid comparison and subject to vectorisation efficiency and memory management effects. Hence, the triangle count of surrogate models decreases with increasing k , i.e. $|\mathbb{T}_k| \ll |\mathbb{T}_{k+1}|$.

Definition 4 A surrogate model $\mathbb{T}_{k_i}(p_i)$ inducing $\mathbb{T}_{k_i}^\epsilon(p_i)$ is conservative if

$$\forall p_i, p_j, k_i, k_j : \mathbb{T}_{k_i}^\epsilon(p_i) \cap \mathbb{T}_{k_j}^\epsilon(p_j) = \emptyset \Rightarrow \mathbb{T}^\epsilon(p_i) \cap \mathbb{T}^\epsilon(p_j) = \emptyset.$$

Conservative means that any two surrogates of two particles are in contact (overlap) if the two particles are in contact. Yet, if their surrogates are in contact, there might still be gaps between the particles, i.e. there might be no contact point.

Corollary 1 Let a surrogate model hierarchy $\mathbb{T}_k(p)$, $k \geq 1$ be monotonous if

$$\forall 1 \leq \hat{k} < k : \forall t_{\hat{k}}^\epsilon \in \mathbb{T}_{\hat{k}}^\epsilon(p) : t_{\hat{k}}^\epsilon \subseteq \bigcup_{t \in \mathbb{T}_k^\epsilon(p)} t.$$

Our surrogate hierarchies do not have to be monotonous.

A monotonous cascade of triangles plus ϵ -environments would grow in space as we move up the hierarchy of models. Therefore, we do not impose it, even though monotonicity would imply conservativeness “for free”. Empirical evidence suggests that abandoning monotonicity allows us to work with significantly tighter ϵ -choices per level. Yet, it also implies that we generally cannot show algorithm correctness through plain induction.

Classic level-of-detail algorithms require a coarsened representation of a triangulated model to preserve certain properties such as connected triangle surfaces or the preservation of certain features such as sharp edges. Our surrogate models however are to be used as temporary replacements within our calculations. We thus can ask for weak representations of the geometries:

Definition 5 The triangles of a particle have to span a connected surface. For surrogate models, there is no such constraint. Therefore, the surrogate models can be weakly connected: Their triangles can be disjoint with gaps in-between or they can intersect each other. A surrogate’s ϵ -environment is connected however, and it covers (overlaps) all connectivity of the original model.

The connectivity addendum in Definition 5 motivates the term weakly connected. It clarifies that we—despite the disjoint, anarchic configuration of a surrogate triangle set (Figure 1)—cannot miss out on some geometry extrema such as sharp edges due to tests with surrogates: If there is no contact between two surrogates, there is also no contact between their real discretisations.

Definition 4 implies that we can use surrogate models as guards and run through them for coarse to fine: If there are no contact points between two surrogate models, there can be no contact points for the more detailed models. We can stop searching for contact points immediately. It does however not hold the other way round. Definition 3 implies immediately that the number of triangles that we examine in such an iterative approach is monotonously growing. Definition 5 gives us the freedom to construct such triangle hierarchies, as it strips us from many geometric constraints.

4.1 Surrogate triangles

The construction of good surrogate models is a challenge of its own, as there are infinitely many surrogate models for a given particle p . We rely a functional minimisation with a fixed

coarsening factor to construct the surrogate hierarchy bottom-up. Let one surrogate triangle for a set of triangles \mathbb{T}_{k-1} be spanned by its three vertices $x_1, x_2, x_3 \in \mathbb{R}^3$ which follow

$$\begin{aligned} \arg \min_{x_1, x_2, x_3} & \frac{1}{\beta_{\text{size}}} \sum_{x \in \{x_1, x_2, x_3\}, t \in \mathbb{T}_{k-1}} \|x - t\|^{\beta_{\text{size}}} + \frac{\alpha_{\text{area}}}{2} |(x_2 - x_1) \times (x_3 - x_1)|^{-2} \\ & + \frac{\alpha_{\text{inside}}}{\beta_{\text{normal}}} \sum_{x \in \{x_1, x_2, x_3\}, x_t \in t \ \forall t \in \mathbb{T}_{k-1}} (\max(0, (x - x_t) \cdot N(x_1, x_2, x_3)))^{\beta_{\text{normal}}}. \end{aligned} \quad (4)$$

$\beta_{\text{size}} \geq 2$ is a fixed integer parameter which we usually pick very high, and the term $\|x - t\|$ denotes the distance between a point x and a triangle t . The sum thus minimises the maximum distance between the vertices of the surrogate triangle and the triangles from \mathbb{T}_{k-1} . We try to make the surrogate triangle as small as possible. The second term acts as a regulariser that avoids that the surrogate triangle degenerates and becomes a single point or a line. Without it, the first term would yield a single point, i.e. $x_1 = x_2 = x_3$.

The third term exploits the fact that each triangle t of p has a unique outer normal $N(t)$. Even though our surrogate models can be weakly connected, it is thus possible to assign each surrogate triangle an outer normal, too. The penalty term over the scalar product drops out due to the max function if the surrogate's normal points into the same direction as the triangles' normals. Effectively, this term ensures that the surrogate triangle nestles closely around a particle and that spikes do not induce a blown-up surrogate (Fig. 2). Once (4) yields a surrogate triangle, ϵ is chosen such that the triangle is conservative for \mathbb{T}_{k-1} .

4.2 Surrogate trees

Algorithm 5 Top-down algorithm to construct a cascade of surrogate models for a given triangulation \mathbb{T} . The algorithm yields a tree defined through $\sqsubseteq_{\text{child}}$ and hence allows us to derive a vast set of different, locally adaptive surrogate models.

```

1: function CONSTRUCTSURROGATE( $\mathbb{T}$ )
2:   Construct surrogate triangle  $t$  for  $\mathbb{T}$  ▷ Solve (4)
3:   Assign  $t$  smallest  $\epsilon$  such that  $t^\epsilon$  is conservative surrogate
4:   Create trivial graph  $\mathcal{T}$  with single node  $\{t^\epsilon\}$  and no edges
5:   CONSTRUCTSURROGATERECURSIVELY( $t^\epsilon, \mathbb{T}$ )
6: end function
7: function CONSTRUCTSURROGATERECURSIVELY( $t_{\text{local}}^\epsilon, \mathbb{T}_{\text{local}}$ )
8:   if  $\mathbb{T}_{\text{local}} \leq N_{\text{surrogate}}$  then
9:     Add node  $\mathbb{T}_{\text{local}}$  to  $\mathcal{T}$ 
10:    Add edge  $\mathbb{T}_{\text{local}} \sqsubseteq_{\text{child}} \{t_{\text{local}}^\epsilon\}$  to  $\mathcal{T}$ 
11:  else
12:    Split  $\mathbb{T}_{\text{local}}$  into  $N_{\text{surrogate}}$  sets  $\mathbb{T}_{\text{local},0}, \mathbb{T}_{\text{local},1}, \mathbb{T}_{\text{local},2}, \dots$  of roughly same size
13:    for  $i$  do
14:      Construct surrogate triangle  $t_{\text{new}}$  for  $\mathbb{T}_{\text{local},i}$  ▷ Solve (4)
15:      Assign  $t_{\text{new}}$  smallest  $\epsilon$  such that  $t_{\text{new}}^\epsilon$  is conservative surrogate over  $\mathbb{T}_{\text{local},i}$ 
16:      Add node  $\{t_{\text{new}}^\epsilon\}$  to  $\mathcal{T}$ 
17:      Add edge  $\{t_{\text{new}}^\epsilon\} \sqsubseteq_{\text{child}} \{t_{\text{local}}^\epsilon\}$  to  $\mathcal{T}$ 
18:      CONSTRUCTSURROGATERECURSIVELY( $t_{\text{new}}^\epsilon, \mathbb{T}_{\text{local},i}$ )
19:    end for
20:  end if
21: end function

```

Let $N_{\text{surrogate}} > 1$ be the surrogate coarsening factor. We construct a surrogate tree top-down (Algorithm 5):

- The first triangle that we insert into \mathcal{T} is the coarsest surrogate model, i.e. a degenerated object description consisting of one triangle. This is the root node of our surrogate tree.
- Recursively dividing creates a tree over sets where all non-leaves have cardinality one. The leaf sets have a cardinality of roughly $N_{\text{surrogate}}$. The number of children per tree node is bounded and typically around $N_{\text{surrogate}}$. Let the root node define the coarsest surrogate model $\mathbb{T}_{k_{\text{max}}}$.

- The union over all leaf sets yields the particle triangulation \mathbb{T}_0 .
- Let the level ℓ of a node, i.e. triangle set, be its distance from the root node in the acyclic graph spanned by \mathcal{T} . The union over all sets with the same level yields a surrogate model $\mathbb{T}_{k_{\max}-\ell}$.
- We construct the surrogate triangles by copying one triangle out of the underlying triangle set. Then, we iteratively minimise the functional (4).
- To obtain surrogates with reasonably small ϵ , we cluster the triangle sets through a tailored k -means algorithm [12]. The subsets $\mathbb{T}_{\text{local},i}$ thus are reasonable compact.

5 Multiresolution contact detection

With our surrogate tree definition, we are in the position to propose a multiscale algorithm for the explicit Euler which utilises the tree as early stopping criterion, and we can, starting from the explicit Euler observation, derive two implicit time stepping algorithms that exploit the multiscale nature of the geometry:

5.1 Explicit Euler

Our explicit Euler exploits the multiscale hierarchy by looping over the \mathcal{T} surrogate levels top down. The tree is unfolded depth-first, and we implement an early stopping criterion: If a surrogate triangle and a triangle set from another particle do not collide, then the children of the surrogate triangle in our triangle tree cannot collide either. The depth-first traversal along this branch of the tree thus can terminate early. The surrogate model used “refines” (unfolds) adaptively.

Algorithm 6 Multiresolution contact detection within explicit time stepping. It compares two particles p_i and p_j given by their surrogate trees $\mathcal{T}(p_i)$ and $\mathcal{T}(p_j)$ with each other.

```

1:  $\mathbb{A}_i \leftarrow \text{root}(\mathcal{T}(p_i)), \mathbb{A}_j \leftarrow \text{root}(\mathcal{T}(p_j))$  ▷ Set of active triangles to check
2: while  $\mathbb{A}_i \neq \emptyset \vee \mathbb{A}_j \neq \emptyset$  do
3:    $\mathbb{A}_{i,\text{new}} \leftarrow \emptyset, \mathbb{A}_{j,\text{new}} \leftarrow \emptyset$ 
4:   for  $t_i \in \mathbb{A}_i, t_j \in \mathbb{A}_j$  do
5:      $c \leftarrow \text{CONTACT}(t_i, t_j)$  ▷ Use context-specific  $\epsilon$  depending on  $t_i, t_j$ 
6:     if  $c = \odot \wedge t_i \in \mathbb{T}_0^\epsilon(p_i) \wedge t_j \in \mathbb{T}_0^\epsilon(p_j)$  then ▷ Not converged on non-surrogate triangles
7:        $c \leftarrow \text{CONTACT}(t_i, t_j)$  ▷ Use comparison-based algorithm this time
8:     end if
9:     if  $c \neq \perp$  then
10:      if  $t_i \in \mathbb{T}_0^\epsilon(p_i) \wedge t_j \in \mathbb{T}_0^\epsilon(p_j)$  then ▷ No surrogate triangles,
11:         $\mathbb{C}(p_i) \leftarrow \mathbb{C}(p_i) \cup \{c\}, \mathbb{C}(p_j) \leftarrow \mathbb{C}(p_j) \cup \{c\}$  ▷ i.e. proper contact point
12:      else ▷ Unfold
13:        if  $t_i \in \mathbb{T}_0^\epsilon(p_i)$  then
14:           $\mathbb{A}_{i,\text{new}} \leftarrow \mathbb{A}_{i,\text{new}} \cup \{t_i\}$ 
15:        else
16:           $\mathbb{A}_{i,\text{new}} \leftarrow \mathbb{A}_{i,\text{new}} \cup \{\hat{t} : \hat{t} \sqsubseteq_{\text{child}} t_i\}$ 
17:        end if
18:        if  $t_j \in \mathbb{T}_0^\epsilon(p_j)$  then
19:           $\mathbb{A}_{j,\text{new}} \leftarrow \mathbb{A}_{j,\text{new}} \cup \{t_j\}$ 
20:        else
21:           $\mathbb{A}_{j,\text{new}} \leftarrow \mathbb{A}_{j,\text{new}} \cup \{\hat{t} : \hat{t} \sqsubseteq_{\text{child}} t_j\}$ 
22:        end if
23:      end if
24:    end if
25:  end for
26:   $\mathbb{A}_i \leftarrow \mathbb{A}_{i,\text{new}}, \mathbb{A}_j \leftarrow \mathbb{A}_{j,\text{new}}$ 
27: end while

```

The concept is realised via a marker in Algorithm 6: Let \mathbb{A} identify a set of active nodes from \mathcal{T} . The union of all sets identified by \mathbb{A} yields all triangles from a particle that participate in collision checks. At the begin of a particle-to-particle comparison, only the particles’ roots are active. From there, we work our way down into finer and finer geometric representations

as long as the surrogate models suggest that there might be some contacts, until we eventually identify real contact points stemming from the finest mesh.

Lemma 1 *The hierarchical algorithm yields exactly the same outcome as our baseline code over sets $\mathbb{T}^\epsilon(p_i)$ and $\mathbb{T}^\epsilon(p_j)$. Algorithm 6 is correct.*

Proof 1 *The argument relies on three properties:*

1. *If a contact point is identified for a surrogate triangle, it is not added to the set of contact points. Therefore, a given active set never identifies artificial/too many contact points.*
2. *A contact point is added if it stems from the comparison of two triangles from the fine grid tessellations which are in the active sets.*
3. *Let two triangles t_i^ϵ and t_j^ϵ yield a contact point. As of Algorithm 5 (or the more generic definition of conservatism for surrogates), they belong to nodes (triangle sets) \mathbb{T}_i and \mathbb{T}_j with $\mathbb{T}_i \sqsubseteq_{\text{child}} \hat{t}_i$ and $\mathbb{T}_j \sqsubseteq_{\text{child}} \hat{t}_j$ in $\mathcal{T}(p_i)$ or $\mathcal{T}(p_j)$, respectively. These surrogates fulfil*

$$t_i^\epsilon \cap t_j^\epsilon \neq \emptyset \Rightarrow \hat{t}_i \cap \hat{t}_j \neq \emptyset.$$

and therefore are replaced in the active set by their children by the Algorithm 1 before the respective algorithm terminates.

The correctness of the algorithm follows from bottom-up induction over the levels of \mathcal{T} : The property holds directly for the finest surrogate levels \mathbb{T}_1 of the tree. Any violation thus has to arise from $\mathbb{T}_k, k \geq 2$ in p_i or p_j . We apply the arguments recursively.

We have two triangle-to-triangle comparison strategies on the table (hybrid and comparison-based) which are robust, i.e. always yield the correct solution. If we employ the comparison-based approach only, the $c = \odot$ condition never holds and the corresponding branch is never executed. Otherwise, our algorithmic blueprint implements the hybrid's fall-back as it automatically re-evaluates the contact search for $c = \odot$. However, it is indeed sufficient to rerun this a posteriori contact search if and only if both triangles stem from the finest triangle discretisation:

Corollary 2 *On the surrogate levels within the tree, it is sufficient to use the (efficient) iterative collision detection algorithm (Algorithm 4, bottom), without falling back to the comparison-based variant.*

Proof 2 *Let $\mathbb{T}(p_i) \cap \mathbb{T}(p_j) \neq \emptyset$, i.e. two particles collide. We assume the lemma is wrong, i.e. the tree unfolding terminates prematurely. This assumption formally means*

$$\exists t_i \in \mathcal{T}(p_i), t_j \in \mathcal{T}(p_j) : r(p_i, p_j) = \perp,$$

with

$$\exists t_{0,i} \in \mathbb{T}(p_i), t_{0,j} \in \mathbb{T}(p_j) : t_{0,i} \sqsubseteq_{\text{child}} \dots \sqsubseteq_{\text{child}} \hat{t}_i \wedge t_{0,j} \sqsubseteq_{\text{child}} \dots \sqsubseteq_{\text{child}} \hat{t}_j \wedge t_{0,i}^\epsilon \cap t_{0,j}^\epsilon \neq \emptyset.$$

This assumption is a direct violation of the definition of a surrogate model which has to be conservative.

5.2 Implicit Euler with multiresolution acceleration

Picard iterations can exploit the multiscale hierarchy by looping over the hierarchy levels top down: Per iteration of Algorithm 3, we have to identify all contact points for the current particle configuration. This search for contact points is the same search as we use it in an explicit Euler. If we replace the contact detection within the inner loop with our multiscale contact detection from Section 5.1, we obtain an implicit Euler where the surrogate concept is used *within the Picard loop* as multiresolution acceleration. The surrogate concept enters the algorithm's implementation as a black-box.

Corollary 3 *An implicit Euler using surrogates within the Picard loop body to speed up the search for contact points yields the same output as a flat implicit code with the same number of Picard iterations.*

Proof 3 *This is a direct consequence of Lemma 1 and implies the algorithm’s correctness.*

Though we end up with exactly the same number of Picard iterations, the individual iterates are accelerated internally by the multiresolution technique: Per Picard step, we expect the surrogate trees’ height times $N_{\text{surrogate}}$ to dominate the compute cost—instead of a plain code’s $N_{\text{surrogate}}^2$.

5.3 Implicit multi-resolution Euler

A more bespoke implicit multiresolution algorithm arises from two ideas inspired by multilevel non-linear equation system solvers. On the one hand, the multiscale Algorithm 5.2 consists of two nested while loops—the outer loop stems from the Picard iterations, the inner loop realises the tree unfolding—which we can permute. We obtain an algorithm that runs top-down via the active sets through the surrogate hierarchies and unfolds the trees step by step. Per unfolding step, it uses the Picard loop to converge on the selected hierarchy level. The rationale behind such a permutation is the observation that the efficiency of a nonlinear equation system solver hinges on the availability of a good initial guess. Surrogate resolution levels might be well-suited to deliver a good initial guess of what \mathbb{T} looks like in the next time step. This train of thought is similar to the extension of multigrid into full multigrid. On the other hand, the same multigrid analogy suggests that we do not have to converge on a surrogate level, as the level supplements only a guess anyway. In the extreme case, it is thus sufficient to run one Picard iteration per unfolding step only.

Our advanced variant of the implicit Euler thus is an *outer-loop multi-resolution Picard scheme*. Let the Picard loop start from the coarsest surrogate representation per particle (Algorithm 7). These representations form our initial active sets. Different to the explicit scheme, we maintain an active set $\mathbb{A}(p_i, p_j)$ per particle-particle combination p_i, p_j : A particle p_i can exhibit a very coarse surrogate representation against one particle, while use a very detailed mesh when we compare it to another one. After the Picard step, any surrogate triangle for which the hybrid algorithm has not terminated or for which we identified a contact point is replaced by its next finer representation in the respective active set combination, i.e. for the particular comparison counterpart. In the tradition of value-range analysis, we widen the active set [?]. The Picard loop terminates if the plain algorithm’s termination criteria hold, i.e. the outcome of two subsequent iterations does not change dramatically anymore, and no surrogate tree node has unfolded anymore throughout the previous iterate.

The algorithm is completed by a clean up which removes “redundant” triangles from the active set and ensures that the set is consistent with the tree: It runs through the active set of a particle-particle combination once again. If any of a surrogate triangle’s children is part of the active set, the surrogate is removed from the set and the routine ensures that all of its children are in the set. If all children of a surrogate triangle do certainly not contribute a contact point anymore, they are thus automatically replaced with their parent surrogate triangle. We narrow the active set. Our algorithm discussion closes with the observation that the number of particle-particle combination is potentially huge yet small in practice, as particles are rigid and thus cannot cluster arbitrarily dense.

Our genuine multiscale formulation stresses the convergence requirements further: While Assumption 1 guarantees the convergence of the Picard iterations on the finest level, our multi-resolution approach may push the solution into the wrong direction via the surrogate levels and thus make the initial guess on the next finer level leave the single level’s convergence domain.

Assumption 2 *We assume that a Picard iteration on any level of the surrogate trees yields a new solution on the same or a finer resolution which remains inside the respective Picard iteration’s region of convergence.*

Algorithm 7 Implicit time stepping algorithm where the Picard and multiresolution loop are intermingled.

```

1:  $\forall p_j \neq p_i \in \mathbb{P} : \mathbb{A}(p_i, p_j) \leftarrow \text{root}(\mathcal{T}(p_i))$  ▷ Active sets are now parameterised over interactions
2: while  $\mathbb{T}^{\text{guess}}(p_i), v^{\text{guess}}(p_i), r^{\text{guess}}(p_i)$  or any  $\mathbb{A}$  change significantly for any  $p_i$  do
3:    $\forall p_j \neq p_i \in \mathbb{P} : \mathbb{A}_{\text{new}}(p_i, p_j) \leftarrow \emptyset, \mathbb{A}_{\text{new}}(p_j, p_i) \leftarrow \emptyset, \mathbb{C}(p_i, p_j) = \emptyset, \mathbb{C}(p_j, p_i) = \emptyset$ 
4:   for  $p_j \neq p_i \in \mathbb{P}$  do
5:     for  $t_i \in \mathbb{A}(p_i, p_j), t_j \in \mathbb{A}(p_j, p_i)$  do
6:        $c \leftarrow \text{CONTACT}(t_i, t_j)$  ▷ Use context-specific  $\epsilon$  depending on  $t_i, t_j$ 
7:       if  $c = \odot \wedge t_i \in \mathbb{T}_h^\epsilon(p_i) \wedge t_j \in \mathbb{T}_h^\epsilon(p_j)$  then ▷ Not converged on non-surrogate triangles
8:          $c \leftarrow \text{CONTACT}(t_i, t_j)$  ▷ Use comparison-based algorithm this time
9:       end if
10:      if  $c \neq \perp \wedge c \neq \odot$  then ▷ Implicit guess
11:         $\mathbb{C}(p_i) \leftarrow \mathbb{C}(p_i) \cup \{c\}, \mathbb{C}(p_j) \leftarrow \mathbb{C}(p_j) \cup \{c\}$ 
12:      end if
13:      if  $c = \perp$  then ▷ Add only parents
14:         $\mathbb{A}_{\text{new}}(p_i, p_j) \leftarrow \mathbb{A}_{\text{new}}(p_i, p_j) \cup \{\hat{t} : t_i \sqsubseteq_{\text{child}} \hat{t}\}$ 
15:         $\mathbb{A}_{\text{new}}(p_j, p_i) \leftarrow \mathbb{A}_{\text{new}}(p_j, p_i) \cup \{\hat{t} : t_j \sqsubseteq_{\text{child}} \hat{t}\}$ 
16:      else ▷ Widen active sets
17:        ... ▷ Compare to Algorithm 6
18:      end if
19:    end for
20:  end for
21:   $\forall p_j \neq p_i \in \mathbb{P} : \mathbb{A}(p_i, p_j) \leftarrow \mathbb{A}_{\text{new}}(p_i, p_j), \mathbb{A}(p_j, p_i) \leftarrow \mathbb{A}_{\text{new}}(p_j, p_i)$ 
22:  for  $p_i \in \mathbb{P}$  do
23:     $(dv, dr) \leftarrow \text{CALCFORCES}(\mathbb{C}(p_i))$ 
24:     $(v^{\text{guess}}, r^{\text{guess}})(p_i) \leftarrow (v, r)(p_i) + \Delta t \cdot (dv, dr)$ 
25:     $\mathbb{T}^{\text{guess}}(p_i) \leftarrow \text{UPDATE}(\mathbb{T}(p_i), v^{\text{guess}}(p_i), r^{\text{guess}}(p_i), \Delta t)$ 
26:  end for
27:  for  $p_j \neq p_i \in \mathbb{P}$  do ▷ Clean-up, i.e.
28:    ... ▷ add siblings
29:     $\forall t, \hat{t} \in \mathbb{A}(p_i, p_j)$  with  $t \sqsubseteq_{\text{child}} \hat{t} : \mathbb{A}(p_i, p_j) \leftarrow \mathbb{A}(p_i, p_j) \cup \{t' \in \mathcal{T}(p_i) : t' \sqsubseteq_{\text{child}} \hat{t}\}$ 
30:     $\forall t, \hat{t} \in \mathbb{A}(p_j, p_i)$  with  $t \sqsubseteq_{\text{child}} \hat{t} : \mathbb{A}(p_j, p_i) \leftarrow \mathbb{A}(p_j, p_i) \cup \{t' \in \mathcal{T}(p_j) : t' \sqsubseteq_{\text{child}} \hat{t}\}$ 
31:    ... ▷ and remove “redundant” parents
32:     $\forall t \in \mathbb{A}(p_i, p_j) : \mathbb{A}(p_i, p_j) \leftarrow \mathbb{A}(p_i, p_j) \setminus \{\hat{t} \in \mathcal{T}(p_i) : t \sqsubseteq_{\text{child}} \hat{t}\}$ 
33:     $\forall t \in \mathbb{A}(p_j, p_i) : \mathbb{A}(p_j, p_i) \leftarrow \mathbb{A}(p_j, p_i) \setminus \{\hat{t} \in \mathcal{T}(p_j) : t \sqsubseteq_{\text{child}} \hat{t}\}$ 
34:  end for
35: end while
36:  $\forall p_i \in \mathbb{P} : \mathbb{T}(p_i) \leftarrow \mathbb{T}^{\text{guess}}(p_i), v(p_i) \leftarrow v^{\text{guess}}(p_i), r(p_i) \leftarrow r^{\text{guess}}(p_i)$ 
37:  $t \leftarrow t + \Delta t$ 

```

In practice, Assumption 2 might require a damping of the Picard iterations with a relaxation parameter $\theta_{\text{Picard}} \leq 1$ such that an iteration update does not overshoot. That is, θ_{Picard} becomes smaller with bigger surrogate levels.

Lemma 2 *If Algorithm 7 terminates and remains within the region of convergence of the Picard iteration, it yields the correct solution, i.e. the solution produced by the flat models without any surrogate hierarchy.*

Proof 4 *We have to study two cases over a triangle combination $(t_{\mathbb{A}}, t_{\mathbb{U}})$ which yields a contact point. First, assume that $(t_{\mathbb{A}}, t_{\mathbb{U}}) \in \mathbb{A}^{(n)}(p_j) \times \mathbb{U}^{(n)}(p_j)$ yields an invalid contact point, i.e. a contact point not found in the baseline iterate $\mathbb{A}_0^{(n)}(p_j) \times \mathbb{U}_0^{(n)}(p_j)$. This can happen as parts of the geometry “pixel up” and introduce coarse surrogates, which overlap with a fine tessellation on the comparison particle. They can wrongly suggest contact. The $t_{\mathbb{A}}$ or $t_{\mathbb{U}}$ that are surrogate triangles are replaced by their children in $\mathbb{A}^{(n+1)}(p_j) \times \mathbb{U}^{(n+1)}(p_j)$. As the tree is of finite depth, this process will eventually terminate and thus stop contributing “invalid” triangle combinations as contact points.*

In the other case, assume that the comparisons within $\mathbb{A}^{(n)}(p_j) \times \mathbb{U}^{(n)}(p_j)$ lack a triangle pair $(t_{\mathbb{A}}, t_{\mathbb{U}}) \in \mathbb{A}_0^{(n)}(p_j) \times \mathbb{U}_0^{(n)}(p_j)$ which contributes a contact point in the plain model. Due to Definition 4 over conservative surrogates,

$$\forall t_{\mathbb{A}} \in \mathbb{A}_0^{(n)}(p_j), \exists \hat{t}_{\mathbb{A}} \in \mathbb{A}^{(n)}(p_j) : t_{\mathbb{A}} \sqsubseteq_{\text{child}} \dots \sqsubseteq_{\text{child}} \hat{t}_{\mathbb{A}} \quad (5)$$

such that \hat{t} yields a contact point. This point is “invalid”, i.e. not found in the baseline and thus covered by the first case. It eventually is removed as the corresponding \hat{t} is replaced by its children. The analogous argument can be made over $t_{\mathbb{U}}$.

Both case distinctions argue over the widening of the search space $\mathbb{A}^{(n)}(p_j) \times \mathbb{U}^{(n)}(p_j)$. The modification of this space by the algorithm implies that the comparison sequence $\mathbb{A}_0^{(n)}(p_j) \times \mathbb{U}_0^{(n)}(p_j)$ has to be changed after the respective modification, too. As we assume that we remain within the region of convergence of the Picard iteration, this harms the convergence speed but does not imply that we diverge. Little additional work is eventually required to handle the narrowing case:

Lemma 3 *If Algorithm 7 remains within the region of convergence of the Picard iteration, it terminates.*

Proof 5 *Our discussion of Lemma 2 assumes a monotonous growth of $\mathbb{A}^{(n)}(p_j) \times \mathbb{U}^{(n)}(p_j)$ and exploits the fact that this search space is finite and bounded. Let $(t_{\mathbb{A}}, t_{\mathbb{U}}) \in \mathbb{A}_0^{(n)}(p_j) \times \mathbb{U}_0^{(n)}(p_j)$ not contribute a contact point. Neither does its parent $(\hat{t}_{\mathbb{A}}, \hat{t}_{\mathbb{U}})$ or $(t_{\mathbb{A}}, \hat{t}_{\mathbb{U}})$, respectively, or any other child of this parent contribute a contact point. $(t_{\mathbb{A}}, t_{\mathbb{U}})$ consequently is replaced by a combination involving its surrogates in $\mathbb{A}_0^{(n+1)}(p_j) \times \mathbb{U}_0^{(n+1)}(p_j)$. The argument applies recursively. Let there be a $m > n + 1$ for which $(t_{\mathbb{A}}, t_{\mathbb{U}})$ has to be taken into account. We know that it will eventually be re-added. While the cardinalities $\|\mathbb{A}^{(n)}(p_j)\|$ and $\|\mathbb{U}^{(n)}(p_j)\|$ are not monotonously growing, they are non-strictly growing between iteration n and m . Furthermore, we know that the error behind the Picard loop has (strictly) diminished between n and m due to contraction property. We do not encounter cycles.*

5.4 Implementation

The multiresolution representation of an object can be computed at simulation startup as a preprocessing step. While we keep the multiresolution hierarchy when particles move and rotate—we simply have to ensure that all triangles including all surrogates are properly rotated and translated—the flattening of sets of triangles from $\mathcal{T}(p)$ into a sequence of coordinates has to be done once per time step, as the triangle coordinates change in each step. It is reasonable to realise this via lazy flattening, i.e. a given set of triangles is mapped onto its flat representation—including the replication of coordinates—upon first request and then cached for the remainder of the time step.

There are two reasons why our multi-resolution algorithms are expected to yield better performance than their baseline without a hierarchy: First and foremost, we expect the number of triangle-to-triangle comparisons to go down despite the fact that we augmented the triangle set with surrogates. The multiscale algorithm iteratively narrows down the region of a particle where contacts may arise from, and thus studies only the area of a particle which potentially is in contact with a neighbour. At the same time, we can pick $N_{\text{surrogate}}$ such that one leaf set cardinality of the surrogate tree fits exactly to the vector unit length and, hence, cache line architecture.

The $N_{\text{surrogate}}$ -argument breaks down for the multiscale algorithms where the coarser tree levels, by definition, do not occupy a complete vector length. Therefore, we do not run triangle-to-triangle comparisons within the tree directly. Instead, we make the tree/triangle traversal collect all comparisons to be made with a buffer. Once we have identified all triangle collisions to be computed, we stream the whole buffer through the vector units. We merge the flattened triangle representations on-the-fly.

6 Results

Lemma 1, Corollary 3, and Lemma 2 clarify that our proposed algorithms do yield the correct results. They however do not validate that they yield these results quicker than a plain, straightforward algorithm. We hence collect runtime results. All experiments are ran on Intel Xeon E5-2650V4 (Broadwell) chips in a two socket configuration with 2×12 cores. They run at 2.4 GHz, though TurboBoost can increase this up to 2.9 GHz. However, a core executing AVX(2) instructions will fall back to a reduced frequency (minimal 1.8 GHz) to stay within the TDP limits [?].

Our node has access to 64 GB TruDDR4 memory, which is connected via a hierarchy of three inclusive caches. They host $12 \times (32 + 32)$ KiB, 12×256 KiB or 12×2.5 MiB, respectively. We obtain around 109 GB/s in the Stream TRIAD [?] benchmark on the node which translates into 4,556 MB/s per core. The node has a theoretical single precision peak performance between 2.4 (non-AVX mode and baseline speed) and 46.4 Gflop/s per core (AVX 2.0 FMA3 with full turbo boost). All of our calculations are ran in single precision. They are translated with the Intel 19 update 2 compiler and use the flags `-std=c++17 -O3 -qopenmp -march=native -fp-model fast=2`, i.e. we tailor them to the particular instruction set.

All presented performance counter data are read out through LIKWID [?]. DEM codes are relatively straightforward to parallelise as their particle-particle interaction is strongly localised: We can combine grid-based parallelism (neighbour cells) with an additional parallelisation over the particle pairs [10]. The load balancing of these concurrency dimensions however remains challenging. As our ideas reduce the comparison cost algorithmically yet do not alter the concurrency character, we stick (logically) to single core experiments to avoid biased measurements due to parallelisation or load balancing overheads. Yet, we artificially scale up the setup by replicating the computations per node over multiple OpenMP threads whenever we present real runtime data or machine characteristics, and then break down the data again into cost per replica per core. This avoids that simple problems fit into a particular cache or that memory-bound applications have exclusive access to two memory controllers.

6.1 Experimental setup

We work with two different experimental setups. In the *two-particles* setup, we study two spherical objects which are set on direct collision trajectory. They bump into each other, and then separate again. The setup yields three computational phases: While the particles approach, there is no collision and no forces act on the particles as we neglect gravity. When they are close enough, the particles exchange forces and the system becomes very stiff suddenly, before the objects repulse each other again and separate. We focus exclusively on the middle phase. Throughout this approach-and-contact situation, the algorithmic complexity of the contact detection is in $\mathcal{O}(|N_{\text{triangles}}|^2)$, as we assume that both particles have the same triangle count.

In the *sphere-on-plate scenario*, we drop a spherical object onto a tilted plate. The particle hits the plate, bumps back in a slightly tilted angle, i.e. with a rotation, and thus hops down the plate. This problem yields free-fall phases which take turns with stiff in-contact situations. Furthermore, the area of the free particles which is subject to potential contacts changes all the time as the particle starts to rotate, and the contacts result from a complex geometry consisting of many triangles compared to a simplistic geometry with very few triangles. The underlying computational complexity is roughly in $\mathcal{O}(N_{\text{triangles}})$.

For the particles, we work exclusively with *sphere-like shapes*, which result from a randomised parameterisation: We decompose the sphere with radius 1 into $N_{\text{triangles}}$ triangles. If not stated otherwise, $N_{\text{triangles}} = 1,280$. The vertices on the sphere which span the triangles are subject to a Perlin noise function, which offsets the vertex along the normal direction of the surface. $\eta_r = 0$ adds no noise and thus yields a perfect, triangulated sphere where all vertices are exactly 1 unit away from the sphere’s origin. Otherwise, the per-vertex radius is from $[1, 1 + \eta_r]$. As we use a hierarchical noise model, a high η_r yields a degenerated shape which retains a relatively smooth surface.

6.2 Surrogate properties

We first assess our surrogate geometry’s properties. Our coarsest surrogate model consists of a single triangle. We compare this triangle’s longest edge (diameter) $d_{k_{\text{max}}}$ plus its corresponding $\epsilon_{k_{\text{max}}}$ value to the radius r_{sphere} of the bounding sphere of the fine grid object (Table 1). For the surrogate hierarchy, we use $|N_{\text{surrogate}}| = 8$ as coarsening factor; a choice we employ throughout the experiments. In this first test, we keep the lowest frequency of the Perlin noise only, i.e. we stretch the sphere along one direction yet eliminate any further bumps or extrusions. With growing η_r , we obtain increasingly non-spherical objects resembling an

Table 1: Different triangle counts $N_{\text{triangles}}$ per spherish object scaled along one axis by a factor of μ . Per setup, we study the top level surrogate which contains one triangle and compare the maximum triangle diameter plus its halo size against the bounding sphere radius.

μ	$N_{\text{triangles}} = 80$		$N_{\text{triangles}} = 320$		$N_{\text{triangles}} = 1,280$		r_{sphere}
	$d_{k_{\text{max}}}$	$\epsilon_{k_{\text{max}}}$	$d_{k_{\text{max}}}$	$\epsilon_{k_{\text{max}}}$	$d_{k_{\text{max}}}$	$\epsilon_{k_{\text{max}}}$	
1.0	0.09	0.49	0.09	0.50	0.08	0.52	0.50
1.2	0.10	0.55	0.10	0.56	0.10	0.56	0.60
1.4	0.34	0.54	0.12	0.65	0.11	0.66	0.70
1.8	0.14	0.84	0.89	0.53	1.35	0.51	0.90
2.6	1.54	0.58	2.24	0.51	2.36	0.52	1.30

ellipsoid. The rationale behind this simplified noise is that we eliminate non-deterministic effects and study the dominant sphere distortion effects.

The combination of $d_{k_{\text{max}}}$ and $\epsilon_{k_{\text{max}}}$ characterises the shape of our coarsest surrogate model. A large diameter relative to a small halo size describes a disc-like object. A small diameter relative to a large halo size describes a sphere-like object. Different triangle counts for the fine grid model allow us to assess the impact of the level of detail of the fine grid mesh onto the resulting coarsest surrogate geometry.

Our surrogate almost degenerates to a point if the underlying triangulated geometry approximates a sphere. It can not totally degenerate as we penalise triangle degeneration in (4). The triangle count approximating a spherical object does not have a significant qualitative or quantitative impact on this characterisation of the coarsest surrogate triangle. Once the triangulated mesh becomes less spherical, the surrogate triangle starts to align with the maximum extension of the fine mesh. It spreads out within the geometry along the geometry’s longest diameter; an effect that is the more distinct the higher the fine geometry’s triangle count. The halo layer $\epsilon_{k_{\text{max}}}$ around the surrogate triangle, which is analogous to a sphere’s radius if the surrogate triangle approaches a point, remains in the order of $r = 0.5$. This is the radius of the original unit sphere ($\eta_r = 0$).

For a close-to-spherical geometry, our volumetric surrogate model never exceeds 135% of the bounding sphere volume ($N_{\text{triangles}} = 1,280$). For the highly non-spherical cases ($\mu = 2.6$) our surrogate volume can be as little as 37% ($N_{\text{triangles}} = 80$) of the simple bounding sphere volume. This advantageous property results from the observation that a growth of $d_{k_{\text{max}}}$ anticipates any extension of the geometry, while the $\epsilon_{k_{\text{max}}}$ ensures that the minimal geometry diameter, which is at least as large as the original sphere, remains covered by the surrogate triangle plus its halo environment.

Observation 1 *For highly non-spherical sets of triangles, our surrogate formalism yields advantageous representations. For spherical observations, it resembles the bounding sphere. This holds for all levels of the surrogate cascade.*

In a surrogate tree, fine resolution tree nodes (surrogate triangles) are characterised by the low triangle count measurements in Table 1 where localised patches are highly non-spherical (large η_r). Surrogate triangles belonging to coarser levels inherit characteristics corresponding to larger $N_{\text{triangles}}$. We conclude that our triangle-based multiresolution approach is particularly advantageous as an early termination criterion (“there is certainly no collision”) on the rather fine surrogate resolution levels within the surrogate tree, or is overall tighter fitting than bounding sphere formalisms for non-spherical geometries.

6.3 Hybrid single level contact detection

Even though our multiscale approach intends to reduce the number of distance calculations, a high throughput of the overall algorithm continues to hinge on the efficiency of the core distance calculation. We hence continue with studies around the explicit Euler where we omit the multiscale hierarchy. We work with the finest particle mesh representation only.

The assessment of the core comparison efficiency relies on our sphere-on-plate and the two-particles setup. They represent two extreme cases of geometric comparisons: With the plane, a complex particle with many triangles hits very few triangles. Even though the plane is presented by few triangles, we asymptotically approach a $|N_{\text{triangles}}| : 1$ comparison. When we collide two particles—we use the same triangle count for both—we obtain a $|N_{\text{triangles}}| : |N_{\text{triangles}}|$ setup.

On the algorithm side, two code variants are on the table: We can run solely run a comparison-based algorithm, or we can use the hybrid code variant which runs four steps of the iterative scheme before it checks if the two last iterates of the contact point differ by more than $C\epsilon_h$ with $C \approx 1$ and $\epsilon_h = 0.01$; relative to a baseline particle diameter of 1.0 subject to added noise. If the difference exceeds the threshold, our algorithm assumes that the code has not converged, and hence reruns the comparison-based code to obtain a valid contact assessment. The comparison-based code variant is 4-way vectorised and relies on Intel intrinsics. The hybrid variant is vectorised over batches of eight packed triangle pairs using an OpenMP `simd` annotation.

Table 2: Particle collision scenario (top) and particle on slope (bottom). We compare a comparison-based realisation against a hybrid realisation. Per setup, we present the time-to-solution ($[t]=\text{ns}$) per Euler step, i.e. one run through all possible triangle combinations, and we augment these data with MFlop/s rates split up into scalar and vectorised contributions. Vector calculations are categorised as 128 bit packed (SSE) or 256 bit packed (AVX) for four and eight simultaneous 32 bit floating point operations respectively. For the hybrid setup, we finally quantify how many triangle pairs had to be checked a posteriori, i.e. as fallback, by the comparison-based algorithm. This runtime is included in the data. All measurements are given as the average per core.

$ N_{\text{triangles}} $	Comparison-based			Hybrid				
	Runtime	Scalar	packed 128B	Runtime	Scalar	packed 128B	packed 256B	Fallback
12	659	0.0152	3,217	499	62.7	1110	10,726	7.7%
36	517	0.0019	3,462	276	127.0	969	14,538	4.5%
140	3,804	0.0003	3,183	1,833	197.2	325	18,402	1.2%
1,224	434,723	0.0000	3,042	199,379	242.1	53	20,950	0.028%
12	26	0.0387	3,325	28	10.6	1,250	9,335	6.3%
36	65	0.0196	3,853	67	15.6	1,339	11,934	5.1%
140	184	0.0128	4,094	179	21.5	1,335	13,488	4.8%
1,224	1,983	0.0029	4,272	1,846	30.3	932	14,794	3.6%

Our hybrid approach outperforms a sole comparison-based approach robustly for the $|N_{\text{triangles}}| : |N_{\text{triangles}}|$ setups. For strongly ill-balanced triangle counts, the insulated comparison-based approach is superior (Table 2). The comparison-based code variant is not able to benefit from AVX at all (not shown), while the hybrid AVX usage increases with increasing triangle counts. We end up with up to 40-45% “turbo-mode” peak performance which we have to calibrate with the AVX frequency reduction [?]. The relative number of fallbacks, i.e. situations where the iterative scheme does not converge within four iterations, decreases with growing geometry detail, while the same effect is not as predominant for the particle-on-plane scenario.

Our data confirm the superiority of the hybrid approach for the particle-particle comparisons [9, 10]. They confirm that the approximation of the Hessian does not significantly harm the robustness, even though the number of fallbacks becomes non-negligible. Our arithmetic intensity dominated by the $\mathcal{O}(|N_{\text{triangles}}|^2)$ for the $|N_{\text{triangles}}| : |N_{\text{triangles}}|$ algorithm in the sphere-to-sphere setup as opposed to $\mathcal{O}(|N_{\text{triangles}}|)$ for sphere-on-plate determines how much improvement results from the hybrid strategy. The latter prospers through vectorisation. We see an increased fallback for decreased geometric detail due to the larger relative epsilon, which is used to identify fallback conditions.

Observation 2 *As long as we do not compare extreme cases (single triangle vs. a lot of triangles), the hybrid approach is faster. It is thus reasonable to employ it on all levels of the*

surrogate tree, even though it might be reasonable to skip iterative comparisons a priori if the coarsest surrogate level is involved. The latter observation does not result from a mathematical “non-robustness” but is a sole machine effect.

6.4 Multiresolution comparisons for explicit time stepping

Table 3: Measurements for an explicit Euler over 100 time steps for the particle-particle collision (top) and the particle-on-plane setup (bottom). We compare a comparison-based setup to a hybrid approach on a single level vs. a surrogate hierarchy which is traversed from coarse to fine. For the hybrid configuration, we show both the number of iterative sweeps of four iterations and the plain triangle-to-triangle comparisons.

Method	Comparison-based		Hybrid		
	#tri. comp.	Runtime	#tri. comp.	#iterative	Runtime
Single level	149,817,600	39.62	165,599	149,817,600	18.68
Surrogate hierarchy	819,926	0.26	14,353	764,336	0.18
Single level	62,668,800	16.80	1,566,414	62,668,800	0.08
Surrogate hierarchy	527,141	7.68	49,584	503,402	0.04

Within an explicit time stepping code, our multiresolution approach promises to eliminate unnecessary comparisons since it identifies “no collision” constellations quickly through the surrogates: Whenever it compares two geometries, the algorithm runs through the resolution levels top-down (from coarse to fine). The monotonicity of the surrogate definition implies that we can stop immediately if there is no overlap between two surrogates. Our code either employs the pure geometry-based approach or the hybrid strategy on all levels.

Our measurements confirm the superiority of the hybrid scheme in the surrogate context (Table 3): In line with Section 6.3, no multiresolution setup with comparison-based contact detections on surrogate levels is able to outperform the configurations where all levels are tackled through the hybrid approach. Further studies where different variants are used on different (surrogate) levels are beyond scope.

In our two-particles scenario, the particles each host 1,224 triangles, and hence yield $1,224^2$ comparisons per time step if no surrogate helper data structure is used. As we sum up the comparisons over 100 time steps, the $\mathcal{O}(|N_{\text{triangles}}|^2)$ complexity delivers exactly the measured total comparison count. An analogous argument holds for the sphere-on-plate setup, where the slope hosts 512 triangles. In both cases, the number of triangle comparisons is reduced by more than an order of magnitude through the surrogate hierarchy, and the surrogate version outperforms its single-level baseline robustly. The hierarchical scheme’s additional computational cost (overhead) is negligible, though it does not significantly alter the ratio of iterative checks to fallback comparisons in the hybrid scheme.

Observation 3 *Our surrogate technique efficiently reduces the number of comparisons between two geometries, as “no-collision” setups are identified with low computational cost.*

6.5 Multiresolution comparisons for implicit time stepping

Implicit methods are significantly more stable than their explicit counterpart. The price to pay for this is an increased computational complexity: The Picard iterations that we use imply that we have to run the core contact point detection more often per time step. The Picard iterations’ update of collision point detections imply that the surrogate tree does not unfold linearly anymore. While the explicit time stepping algorithm runs through the tree from coarse to fine, the implicit scheme descends into finer levels yet might, through the iterative updates of the rotation and position, find alternative tree parts that have to be taken into account too or instead.

Once we study the comparisons over 100 time steps, we observe that the number of Picard iterations is small and bounded (Table 4). We study the impact of a switch to the iterative scheme, with the hybrid fallback on the finest level, and observe that it slightly increases the

Table 4: Average number of Picard iterations per time step for our first two scenarios.

Method	Particle-particle		Sphere-on-plate	
	Comparison-based	Iterative	Comparison-based	Iterative
Single level or surrogate within Picard	4.6	4.9	7.1	7.1
Multiscale Picard	6.2	6.2	13.0	13.1

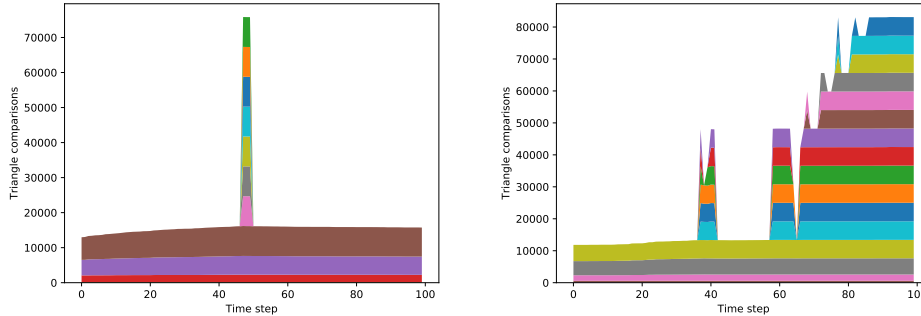


Figure 3: Number of triangle-to-triangle comparisons over time per surrogate representation level. The data stems from the particle-particle collision (left) and the particle-slope setup (right) subject to the implicit time stepping.

Picard iteration count. The usage of a multiscale method merged into the Picard iterations increases the iteration count, too. Both modifications yield flawed contact point guesses and thus require us to run more Picard iteration steps overall. The wrong guesses have to be compensated later on.

Observation 4 *Both the iterative approximation of contact points and the “one Picard step before we widen the active set” strategy increase the total number of required Picard iterations.*

The surrogate hierarchy yields an efficient early termination criterion for our collision detection. If there is no collision, the code does not step down into the fine grid resolutions. This property carries over from the explicit to the implicit algorithm (Figure 3). An increase of the computational cost by a factor of 4.6 is acceptable in return for an implicit scheme. We however observe that this increase holds for brief point contacts only. It raises to a factor of 13.1 if contacts persist. In our example, this happens once the spherical object starts to roll and slide down the tilted plane.

Table 5: Measurements for our implicit schemes for the particle-particle collision (top) and the particle-on-plane setup (bottom).

Method	Comparison-based		Hybrid		
	#tri. comp.	Runtime	#tri. comp.	#iterative	Runtime
Single level	689,160,960	169.16	878,435	734,106,240	74.42
Surrogate within Picard	3,971,099	1.08	71,365	3,697,147	0.72
Multiscale Picard	1,816,493	0.77	22,481	1,699,106	0.47
Single level	443,068,416	96.06	11,081,636	443,695,104	44.10
Surrogate hierarchy	3,590,702	0.48	344,087	3,421,174	0.22
Multiscale Picard	3,503,405	0.49	310,982	3,351,022	0.19

Within our multi-resolution framework, the cost per Picard iteration is not uniform and constant but depends heavily on the surrogate tree fragments that are used. The cost are in particular non-uniform for non-simplistic setups. The growth in Picard iterations (on average)

per time step (Table 4) increases the number of triangle-to-triangle checks, compared to the explicit schemes (Table 3), by exactly this factor if we stick to a plain geometry model. Yet, it does not manifest in an explosion of the runtime (Table 5) if we employ the surrogate trees. They help to reduce the compute cost dramatically, as we study only those parts of the surrogate tree which might induce a collision. We prune the tree per Picard iteration.

Observation 5 *Our multiscale Picard approach is particularly beneficial for strongly stationary setups where the topology of particle interactions changes quickly.*

Permuting and fusing the Picard iteration loops and the traversal over the surrogate tree reduces the number of triangle-to-triangle comparisons further. This observation holds for the particle-particle setup. It does not hold for the particle-on-plane. The advanced version benefits from the fact that we memorise the active set in-between two Picard iterations: While the implicit version from Section 5.2 runs through the whole tree starting from the root in every iteration, our advanced version starts from a certain resolution and unfolds at most one level per Picard step. We save the progress through coarser resolutions, and we do not step all the way down in early iterations. This state-based approach works as our narrowing is effective: if we step down into a “wrong” part of the tree and find out that these fine resolutions do not contribute towards the final force, we successively remove these fine resolutions from the (active) comparison sets again. For a sphere rolling or hopping down a plane, the active set remains almost invariant throughout the Picard iterations, and we do not benefit from the narrowing or an early termination. We do however benefit here from the adaptive localisation of the contact detection within the tree.

Observation 6 *The multiscale Picard approach in combination with a hybrid contact detection keeps the cost of the implicit time stepping bounded by a factor of four compared to an explicit scheme.*

7 Conclusion

We present a family of multi-resolution contact detection algorithms that exhibit low computational cost and high vectorisation efficiency. Few core ideas guide the derivation of these algorithms: We rigorously phrase the underlying mathematics in a multi-resolution and multi-model language where low-cost resolutions (surrogates) or algorithms (iterative contact search) precede an expensive follow-up step which becomes cheaper through good initial guesses or can be skipped in many cases. We replace dynamic termination criteria behind iterative algorithms with fixed iteration counts. While this might induce that we terminate prematurel in some cases, a fixed iteration count allowed us to unroll loops and to permute them. The permutation of loops finally is our last ingredient which we apply on multiple levels: We switch the traversal of triangles with Newton iterations, and we switch the Picard iterations with the tree unfolding.

The present work is solely algorithmic and has theoretical character. A natural next step is its application to large-scale, massively parallel simulations. Furthermore, we rely—so far—on a naive assumption that the Picard iterations converge. A more robust code variant would either identify non-convergence via force, rotation and movement deltas that do not decrease over the Picard iterations, or it would exploit the fact that we know how accurate our surrogate models are via their ϵ value. In both cases, surrogate levels could be skipped automatically.

On the methodological side, there are three natural extensions of our work: First, our surrogate mechanism always kicks off from the surrogate tree’s root when it searches for contact points. For time stepping codes, this is not sophisticated. It might be advantageous to memorise the tree configurations in-between two subsequent time steps and thus to exploit the fact that many particle configurations change only smoothly in time. Second, we work with multiple spatial representations, i.e. accuracies, but we stick to single precision all the way through. It is a natural extension to make our iterative algorithm use a reduced precision on coarse surrogate models, i.e. early throughout the algorithm. Any machine im-precision can be recovered in our case through a slight increase of ϵ . Such a mixed precision strategy

is particularly attractive in an era where more and more compute devices are equipped with special-purpose, reduced-precision linear algebra components. Finally, we next will have to tackle large-scale systems implicitly: DEM models are notoriously stiff, yet the stiffness is localised, as not all particles in a setup typically do interact with all other particles. It is a natural extension to investigate into local time stepping where each particle advanced with its own Δt , and to make the surrogate representations naturally follow and inform these local time step choices.

Acknowledgements

This work made use of the facilities of the Hamilton HPC Service of Durham University.

References

- [1] T. AKENINE-MILLER, E. HAINES, AND N. HOFFMAN, *Real-Time Rendering, Fourth Edition*, A. K. Peters, Ltd., USA, 4th ed., 2018.
- [2] G. BAREQUET, B. CHAZELLE, L. J. GUIBAS, J. S. MITCHELL, AND A. TAL, *Boxtree: A hierarchical representation for surfaces in 3d*, Computer Graphics Forum, 15 (1996), pp. 387–396, <https://doi.org/https://doi.org/10.1111/1467-8659.1530387>, <https://onlinelibrary.wiley.com/doi/abs/10.1111/1467-8659.1530387>, <https://arxiv.org/abs/https://onlinelibrary.wiley.com/doi/pdf/10.1111/1467-8659.1530387>.
- [3] H. DAMMERTZ, J. HANIKA, AND A. KELLER, *Shallow bounding volume hierarchies for fast simd ray tracing of incoherent rays*, Comput. Graph. Forum, 27 (2008), pp. 1225–1233, <https://doi.org/10.1111/j.1467-8659.2008.01261.x>.
- [4] C. EISENACHER, G. NICHOLS, A. SELLE, AND B. BURLEY, *Sorted deferred shading for production path tracing*, Computer Graphics Forum, 32 (2013), <https://doi.org/10.1111/cgf.12158>.
- [5] C. ERICSON, *Real-Time Collision Detection*.
- [6] S. GOTTSCHALK, M. LIN, AND D. MANOCHA, *Obbtree: A hierarchical structure for rapid interference detection*, Computer Graphics, 30 (1997), <https://doi.org/10.1145/237170.237244>.
- [7] M. HELD, J. KLOSOWSKI, AND J. MITCHELL, *Real-time collision detection for motion simulation within complex environments*, in SIGGRAPH '96, 1996.
- [8] K. IGLBERGER AND U. RÜDE, *Massively parallel granular flow simulations with non-spherical particles*, Computer Science - Research and Development, 25 (2010), pp. 105–113, <https://doi.org/10.1007/s00450-010-0114-4>.
- [9] K. KRESTENITIS AND T. KOZIARA, *Calculating the minimum distance between two triangles on simd hardware*, 4 2015.
- [10] K. KRESTENITIS, T. WEINZIERL, AND T. KOZIARA, *Fast dem collision checks on multicore nodes.*, in Parallel processing and applied mathematics : 12th International conference, PPAM 2017, Lublin, Poland, September 10-13; revised selected papers. Part 1., R. Wyrzykowski, J. J. Dongarra, E. Deelman, and K. Karczewski, eds., no. 10777 in Lecture Notes in Computer Science, 2018, pp. 123–132.
- [11] T. Y. LI AND J. S. CHEN, *Incremental 3D collision detection with hierarchical data structures*, Proceedings of the ACM symposium on Virtual reality software and technology 1998 - VRST '98, 1998 (1998), pp. 139–144, <https://doi.org/10.1145/293701.293719>.

- [12] J. B. MACQUEEN, *Some methods for classification and analysis of multivariate observations*, 1967.
- [13] A. D. RAKOTONIRINA AND A. WACHS, *Grains3D, a flexible DEM approach for particles of arbitrary convex shape - Part II: Parallel implementation and scalable performance*, Powder Technology, 324 (2018), pp. 18–35, <https://doi.org/10.1016/j.powtec.2017.10.033>, <https://doi.org/10.1016/j.powtec.2017.10.033>.
- [14] E. SHELLSHEAR AND R. YTTERLID, *Fast distance queries for triangles, lines, and points using sse instructions*, Journal of Computer Graphic Techniques, 3 (2014), p. 86–110.